First-principles study of 3*sp* impurity (S, P, Si, Al) effects on vacancy-mediated diffusion in Ni and Ni-33Cr alloys

Jia-Hong Ke[1,2*] and Julie D. Tucker[1]

[1] Oregon State University, 204 Rogers Hall, Corvallis, OR 97331

[2] Idaho National Laboratory, 955 MK Simpson Boulevard, Idaho Falls, ID 83415

Abstract

The effect of minor impurities on vacancy-mediated processes is a critical factor causing unanticipated degradation rates in structural alloys. We investigate the 3*sp* impurity effect by first-principles calculations to derive impurity-modified diffusion in dilute Ni. Calculations are also performed for special quasi-random structures (SQSs) of Ni-33Cr to investigate the similarity of representative hops that affect vacancy-mediated kinetics. The results show considerable enhancement of vacancy mobility by P and S for Ni and Ni-Cr alloys due to vacancy binding and reduced migration barriers of the re-orientation hops at the vicinity of the impurity atom. The enhanced diffusion can cause variability of microstructure changes and degradation rates in industrial Ni-based alloys, particularly for structural components where local segregation of impurities can occur due to non-equilibrium conditions.

Keywords: 3*sp* impurities, solute-enhanced diffusion, density functional theory, five-frequency model, quasi-random structure

* Corresponding author at: Idaho National Laboratory, 955 MK Simpson Boulevard, Idaho Falls, ID 83415

E-mail address: jiahong.ke@inl.gov

Nickel-based alloys with concentrated Cr composition have been used as a broad spectrum of structural materials in power industries due to the good combination of corrosion resistance and mechanical strength [1–3]. The industrial alloys of this class such as Alloy 690, 625, and 718 typically have a Cr composition of 17-30 wt.%. Despite the long-established use of these concentrated Ni-Cr alloys, effects of minor impurities on vacancy mediated processes are not comprehensively clarified. The lack of data can be attributed to experimental and modeling challenges, including the time and cost of diffusivity measurements as well as the chemical complexity in modeling concentrated alloys. Although the effect of minor impurities in concentrated Ni-Cr alloys might be semi-quantitatively estimated by using trends observed from dilute Ni (either experimentally or theoretically), this approximation is rarely justified by systematic comparisons. One important influence of minor impurities is the ability to change vacancy mobility, which can either be owing to vacancy trapping by impurity atoms or modified atomic hop frequencies in the vicinity of vacancy-impurity pairs. The impurity effect on vacancy-mediated processes is particularly critical for alloys used for low-temperature and long-term service (e.g. nuclear power system), where defect-impurity interaction is a key factor determining the kinetics of materials degradation.

In this work we focus on the dilute 3*sp* impurities (Al, Si, P, and S). These elements are common impurities in industrial Ni-Cr that are either deliberately added in a minor amount (Al and Si), or residual nonmetals that are detrimental to the mechanical properties (P and S). For industrial Ni-Cr alloys such as Alloy 625 and 718, the composition levels of Si and Al are typically between 0.2 and 0.8 wt.% or less than 1.0 wt.%, whereas the compositions of P and S must be controlled below 0.015 wt.%. There has been a wide body of theoretical research on the impurity diffusion in dilute fcc Ni using first-principles density function theory (DFT) calculations and multi-frequency diffusion model [4–9]. However, only a few of them performed thorough investigations of vacancy-impurity interaction and modified vacancy mobility, and studies to explore those in concentrated Ni-Cr are even lacking. Recent first-principles studies by Lomaev *et al*. [6] and Ke *et al*. [10] showed considerable enhancement of vacancy mobility by very dilute sulfur and phosphorus in fcc Ni. The latter study further showed that the necessary features to enhance vacancy mobility (pair inversion and re-orientation) remained valid in the simulated special quasi-random structure of Ni-33 at.% Cr with P [10].

Here we performed systematic DFT calculations with Vienna *Ab initio* Simulation Package (VASP) [11,12] and Climbing image nudged elastic band (CI-NEB) calculations [13,14] to investigate the 3*sp* impurity effect on vacancy diffusion in dilute Ni and concentrated Ni-33 at.% Cr. Following the previous studies [5,10,15], all calculations were spin-polarized and the plane wave energy cutoff was selected to be 479 eV. We adopted the treatment from ref. [16] by assuming that the initial magnetic moments of Ni, Cr, and 3*sp* impurity atoms are respectively +1, −1, and +1 μB. The interactions between ions and core electrons are described by the projector augmented wave method [17,18] and the Perdew-Burke-Ernzerhof [19] parameterization of the generalized gradient approximation was used for the exchange correlation potentials. The simulation cells for dilute Ni and Ni-33 at.% Cr are respectively 3×3×3 and 2×2×2 supercells of the fcc conventional lattice, respectively. The binding energy and Bader charge were calculated by the same method as ref. [10]. Climbing image nudged elastic band (CI-NEB) calculations [13,14] were performed to determine the transition state and migration barrier. In all CI-NEB runs, the break condition of energy convergence for electronic relaxation is 10^{-5}–10^{-6} eV and that of force for ionic relaxation is 0.01 eV/Å. For Ni alloys with dilute impurities, the five-frequency model [20–22] was used to calculate the impurity-modified vacancy diffusion coefficient as a function of composition and temperature, and the transition state theory was utilized to calculate the effective jump frequency following the methods in previous studies [8,10]. For the concentrated Ni-33 at.% Cr, CI-NEB calculations of special quasi-random structures (SQS) were implemented to obtain the migration barriers of inversion and re-orientation hops, which are respectively analogous to exchange (ω_2) and rotation (ω_1) hops in the five frequency model. In this way, the featured hops associated with the solute-modified vacancy diffusion can be examined individually. For each impurity in Ni-33 at.% Cr, calculations for three different SQSs, generated by Alloy Theoretic Automated Toolkit (ATAT) [23], were performed to clarify the consistent trend of impurity effects. Note that it is computationally demanding to complete the DFT and NEB calculations of the 3×3×3 supercell of SQS Ni-33 at.% Cr using the consistent condition of energy convergence for electronic relaxation as that of dilute Ni supercells. Due to the possibility of deviation from the transition state caused by local distortion, the complete relaxation in NEB calculations is difficult to achieve, and therefore the transition state and its energy determined by a series of iterative NEB runs will not be fully converged. The 2×2×2 supercell were thus used for the calculations of SQS

Ni-33 at.% Cr. Since the migration barrier is predominantly affected by the shells of atoms decorating from the close vicinity of the solute-vacancy pair [24,25], the migration barrier calculations using a 2×2×2 supercell can capture the dominant effect of local chemical environments. The effect of the supercell size on the calculated migration barrier in dilute Ni was tested by Tucker [15] and Hargather *et al*. [4]. Both studies suggested that the calculated migration barriers using a 2×2×2 supercell are consistent with those calculated by larger supercells.

Figure 1 (a)-(d) shows the temperature dependence of solvent Ni diffusion coefficient in Ni-X alloys with various solute contents up to 1 at.%, where X is the 3*sp* solute elements. The result is calculated by using the solvent enhancement factor derived by Nastar [26], which requires accurate thermo-kinetic energetics calculated by DFT. The calculated vacancy-impurity binding energy, migration barriers and attempt frequencies of the five-frequency model are summarized in Supplementary Information (SI) Section S1, and the calculation of solvent enhancement factor is described in SI Section S2. It is demonstrated in Figure 1 that 3*sp* impurities such as P and S can accelerate the solvent diffusion significantly even by a minor amount less than 0.1 at.%, whereas Al and Si with a maximum of 1 at.% produce very limited effect on solvent diffusion. The pronounced discrepancy of impurity-modified solvent diffusion between P or S and Si or Al can well be explained by the diffusion by vacancy-impurity pairs. The pair mobility can be evaluated by the vacancy-impurity binding and migration barriers of exchange (ω_2) and rotation hops (ω_1) at the vicinity of the impurity atom. Both P and S possess strong vacancy-impurity binding and produce a significantly lower migration barrier of rotation and exchange hops compared to solvent diffusion of Ni, thereby enhancing the vacancy mobility by vacancy-impurity pairs. The barriers of rotation and exchanges hops at the vicinity of P and S are both at least 0.30 eV lower than solvent diffusion. The extreme low migration barrier of sulfur-vacancy exchange (0.24 eV) is consistent with the previous study [6]. For Si and Al, while the barrier of each vacancy-impurity exchange hop is also evidently lower than that of solvent diffusion, the rotation of a vacancy around the impurity and vacancy binding are both energetically unfavorable compared to that of P and S. The vacancy-impurity pair is relatively difficult to form and not mobile, and thus the effect of Si and Al on solvent diffusion is minor as shown in Figure 1 (c) and (d). Note that the impurity-enhanced solvent diffusion follows the relative order of S > P > Si > Al, which is similar to that of impurity diffusion coefficients, as

shown in SI Section S3. The trend is consistent with the general understanding that fast diffuser by the vacancy mechanism can accelerate the diffusion of solvent atoms.

To characterize and clarify the impurity effect on vacancy mobility, Figure 2 (a)-(d) shows the temperature dependence of the effective vacancy diffusion coefficient $D_{\mathrm{v}}^{\mathrm{eff}}$ in Ni-X alloys with various impurity compositions. Note that the same DFT results calculated in [10] were used for the plots of diffusion coefficients in Figure 1 (a) and Figure 2 (a). The plots of diffusion coefficients of free vacancies ($D_{\mathrm{v}}^{\mathrm{free}}$) and vacancy-solute pairs ($D_{\mathrm{v}}^{\mathrm{pair}}$) are manifested as the two limits of vacancy transport (see [10,27,28] for detailed information on the calculation). It is shown that for P and S, increasing the solute composition or decreasing temperature makes $D_{\mathrm{v}}^{\mathrm{eff}}$ approach to the limit of vacancy-solute pairs, and $D_{\mathrm{v}}^{\mathrm{pair}}$ is significantly larger than $D_{\mathrm{v}}^{\mathrm{free}}$ for most temperatures due to the low migration barriers of exchange and rotation hops. This non-Arrhenius feature indicates a change of diffusion mechanism from free vacancies to vacancy-impurity pairs as temperature decreases and impurity composition increases. The feature is also shown for Si at low temperature in a very slight degree (Figure 2(c)) since the vacancy binding is relatively moderate (−0.11 eV). As shown in Figure 2 (d), diffusion for fcc Ni alloyed with Al is governed by free vacancies at the whole temperature range due to the weak vacancy binding (−0.04 eV), and the vacancy-Al pair diffusion is not an efficient mechanism because of the higher ω_1 (rotation) barrier than ω_0. Note that in fcc Ni with 1 at.% P or S, vacancy diffusion is predominantly governed by vacancy-impurity pairs at temperatures lower than 1000 K, as seen in Figure 2 (a) and (b).

The analysis shows that the vacancy-impurity binding, rotation (re-orientation or ω_1-type) hops, and exchange (inversion or ω_2-type) hops are the three key factors determining the impurity-modified vacancy-mediated process and contribution of vacancy-solute pairs in vacancy mobility. To clarify the effect of impurities on the concentrated Ni-Cr alloys in comparison with the dilute Ni alloys as describe above, these three characteristics were evaluated by DFT calculations of 3 different special quasi-random structures of the 2×2×2 fcc supercell consisting of 20 Ni atoms, 10 Cr atoms, one impurity atom, and a vacant site. The SQSs were generated by ATAT [23] seeking the best match of correlation functions as a random alloy considering the first two nearest-neighbor shells of pairs and triplets. Note that the structure each containing a first nearest-neighbor vacancy-impurity pair was selected manually during the Monte Carlo searching of SQS. By doing so the 20Ni-10Cr-1X-1Vac SQS can be used to

calculate vacancy-impurity binding energy and migration barriers of rotation and exchange hops at the vicinity of the impurity X. Note that for each 20Ni-10Cr-1X-1Vac quasi-random structure, there are four distinctive rotation hops around the impurity, as shown by the highlighted atoms (including 3 Ni atoms and 1 Cr atom) in the SQS configuration shown in Figure 3 (a). The effect of impurity on vacancy kinetics can then be manifested by comparing the associated migration barriers in 20Ni-10Cr-1X-1Vac SQS to the same structure but with the impurity atom replaced by Ni or Cr in an averaged manner.

Figure 3 (b) shows the mean vacancy binding energies of 3*sp* impurities in the 20Ni-10Cr-1X-1Vac quasi-random structures, along with the vacancy binding in dilute Ni alloys for comparison. The detailed calculation results for each quasi-random structure are summarized in SI Section S4 and S5. The strength of vacancy binding in the concentrated SQS generally follows the same trend as that in dilute Ni alloys. For P, S, and Si, the mean binding energies are in similar magnitude as that in dilute Ni, while it is found that Al in the concentrated SQS demonstrates stronger vacancy binding (−0.14 eV) compared to dilute Ni (−0.04 eV). The change of migration barrier caused by the 3*sp* impurity atom is shown in Figure 3 (c), where ω_2 represents the exchange or inversion type of migration between the impurity atom and vacancy, and ω_1_Cr and ω_1_Ni represent the rotation or re-orientation type of hops of the Cr or Ni atom, respectively. The mean migration barriers of impurity-vacancy exchanges of all 3*sp* solutes are evidently smaller than that of Cr or Ni in the concentrated SQS, particularly for P, S, and Al, while the vacancy-Si exchange barrier is comparable to that of the matrix atoms. For the re-orientation type of hops, P and S impurities consistently decrease the migration barrier by ~0.1-0.3 eV for all the 12 calculated rotation barriers considered in the 3 different Ni-33Cr quasi-random structures. On the other hand, Si produces relatively minor influence on most of the re-orientation hops, while Al increases the mean re-orientation barrier with a wide standard deviation. Note that due to the moderate vacancy-Al binding in the concentrated SQS and the increased re-orientation barrier, Al may be able to trap vacancies and reduced the overall mobility in Ni-33Cr. This is unlikely to happen in dilute Ni because of the weak vacancy-Al binding in dilute Ni.

The calculated vacancy binding energies and migration barriers of exchange and re-orientation hops in the Ni-33Cr quasi-random structure clearly demonstrate consistent trends among P, S, and Si impurities compared to those in dilute Ni. The vacancy binding and modified

kinetic energetics by these impurities are quantitatively consistent between dilute Ni and averaged Ni-33Cr SQS. Note that the calculations for the concentrated SQS are considered static configurations, so the effects of diffusion correlation and the evolution of atomic configurations such as that during local ordering or clustering were not taken into account. Robust simulations of vacancy-mediated processes in concentrated alloys would require more advanced methods to construct accurate energetics by an effective Hamiltonian description of activation energies [29,30].

The predicted impurity effect on vacancy kinetics has provided a fundamental understanding of P-accelerated Ni_2Cr ordering that contributes to the unexpected acceleration of hardening of Ni-Cr commercial and model alloys [31–33]. In this study we further demonstrate that both P and S can produce a similar enhanced effect on vacancy mobility by promoting strong vacancy-impurity complexes with remarkably-reduced migration barriers. In contrast, atom transport by vacancy-impurity complexes for other 3*sp* impurities (Al and Si) is inefficient due to the small reduction or even increase of re-orientation barrier compared to the counterpart without impurities. The prediction of the Si impurity effect is in qualitative agreement with the recent experimental study [34], showing negligible effect of Si on Ni_2Cr hardening kinetics in Ni-33Cr alloys with either low or high levels of Si (0.01 and 0.28 wt.%) at temperatures between 373 and 470 °C.

In addition to thermo-kinetic energetics, the similarity of 3*sp* impurity effects between dilute Ni and concentrated SQS can also be perceived by the analysis of charge distribution at the vicinity of impurities. Table 1 shows the calculated Bader charges of the 3sp impurity atoms in the dilute Ni and concentrated SQS at the ground state and transition state of the rotation and exchange hops. The Bader analysis of dilute Ni shows that P and S have negative Bader charges, whereas Al and Si have positive charges. Al particularly has a large positive Bader charge of ~1.8-1.9*e*, which is consistent with the recent study [6]. These results indicate that both P and S attract valence electrons from the Ni solvent atoms, whereas Si and Al donate electrons to the solvent atoms. The consistent feature of Bader charges among these 3*sp* impurities can be found in the concentrated SQS, as demonstrated in Table 1. One notable discrepancy is that P and S attract more electrons from solvent atoms in the concentrated SQS compared to dilute Ni, and Si and Al donate fewer electrons to solvent atoms. Note that we observed no correlations between migration barrier and Bader charges of 3*sp* impurities (particularly comparing Al and Si), which

is not consistent with the study [6] suggested. While the Bader charge may be a good indicator for comparing the strength of vacancy-solute binding or electron sharing, the magnitude of migration barrier is synergistically associated with the chemical/size effect and the change of the first-neighbor coordinate number, and thus the trend of migration barrier among different impurities may not be well captured by simple characteristics of impurity atoms.

In summary, we have employed the first-principles calculations to predict the modified solvent diffusion and vacancy mobility by the addition of dilute 3*sp* impurities in both dilute Ni and concentrated Ni-33Cr alloys. We observed consistent trends of vacancy-solute binding, change of migration barrier, and Bader charges of impurity atoms between dilute Ni and concentrated SQS. The results show a significant enhancement of vacancy mobility by adding a dilute amount of P and S, predominantly due to vacancy binding and remarkably reduced rotation barrier and exchange barrier at the vicinity of P and S atoms. First-principles calculations of three distinctive quasi-random Ni-33Cr alloys display a strong resemblance between dilute Ni and Ni-33Cr SQS for P, S, and Si. Both P and S enhance the mobility of vacancy-impurity pairs with high hopping frequencies of rotation (re-orientation) and exchange (inversion) jumps. Note that the enhanced diffusion by P or S can cause the variability of microstructure changes and degradation rates in industrial alloys, particularly for structural components where local segregation of impurities can occur due to non-equilibrium conditions. In contrast, Si produces minor influence on vacancy-mediated processes due to the moderate-weak vacancy binding and less-affected migration barriers, and Al may trap vacancies due to the stronger vacancy binding in the concentrated SQS than that in dilute Ni and the higher re-orientation barrier.

Acknowledgements

This material is based upon work supported by the National Science Foundation under Grant No. 1653123-DMR. This research is being performed using funding received from the DOE Office of Nuclear Energy's Nuclear Energy University Program, Cooperative Agreement Number DE-NE0008423.

Data availability

The raw/processed data required to reproduce these findings cannot be shared at this time due to technical or time limitations. The data can be obtained by contacting the corresponding author.

References

[1] S.J.Zinkle, G.S.Was, Acta Mater. 61 (2013) 735–758.

[2] Electric Power Research Institute, Critical Issues Report and Roadmap for the Advanced Radiation-Resistant Materials Program, 2012.

[3] T.M.Pollock, S.Tin, J. Propuls. Power 22 (2006) 361–374.

[4] C.Z.Hargather, S.Shang, Z.Liu, Acta Mater. 157 (2018) 126–141.

[5] J.D.Tucker, R.Najafabadi, T.R.Allen, D.Morgan, J. Nucl. Mater. 405 (2010) 216–234.

[6] I.L.Lomaev, D.L.Novikov, S.VOkatov, Y.N.Gornostyrev, A.Cetel, M.Maloney, R.Montero, S.F.Burlatsky, Acta Mater. 67 (2014) 95–101.

[7] I.L.Lomaev, D.L.Novikov, S.VOkatov, Y.N.Gornostyrev, S.F.Burlatsky, J. Mater. Sci. 49 (2014) 4038–4044.

[8] H.Wu, T.Mayeshiba, D.Morgan, Sci. Data 3 (2016) 1–11.

[9] S.Schuwalow, J.Rogal, R.Drautz, J. Phys. Condens. Matter 26 (2014).

[10] J.-H.Ke, G.A.Young, J.D.Tucker, Acta Mater. 172 (2019) 30–43.

[11] G.Kresse, J.Hafner, Phys. Rev. B 47 (1993) 558–561.

[12] G.Kresse, J.Furthmüller, Phys. Rev. B - Condens. Matter Mater. Phys. 54 (1996) 11169–11186.

[13] G.Henkelman, B.P.Uberuaga, H.Jónsson, J. Chem. Phys. 113 (2000) 9901–9904.

[14] G.Henkelman, B.P.Uberuaga, H.Jónsson, J. Chem. Phys. 113 (2000) 9901–9904.

[15] J.D.Tucker, Ab Initio-Based Modeling of Radiation Effects in the Ni-Fe-Cr System, University of Wisconsin-Madison, 2008.

[16] J.S.Wróbel, D.Nguyen-Manh, M.Y.Lavrentiev, M.Muzyk, S.L.Dudarev, Phys. Rev. B 91 (2015) 024108.

[17] D.Joubert, Phys. Rev. B - Condens. Matter Mater. Phys. 59 (1999) 1758–1775.

[18] P.E.Blöchl, Phys. Rev. B 50 (1994) 17953–17979.

[19] J.P.Perdew, K.Burke, M.Ernzerhof, Phys. Rev. Lett. 77 (1996) 3865–3868.

[20] A.D.LeClaire, J. Nucl. Mater. 69–70 (1978) 70–96.

[21] A.B.Lidiard, London, Edinburgh, Dublin Philos. Mag. J. Sci. 46 (1955) 1218–1237.

[22] A.D.LeClaire, A.B.Lidiard, Philos. Mag. 1 (1956) 518–527.

[23] A.van deWalle, P.Tiwary, M.deJong, D.L.Olmsted, M.Asta, A.Dick, D.Shin, Y.Wang, L.-Q.Chen, Z.-K.Liu, Calphad 42 (2013) 13–18.

[24] Dane Morgan, Ab Initio Based Modeling of Radiation Effects in Multi-Component Alloys:

Final Scientific/Technical Report, Idaho Falls, ID (United States), 2010.
[25] J.G.Goiri, S.K.Kolli, A.Van DerVen, Phys. Rev. Mater. 3 (2019) 1–12.
[26] M.Nastar, Philos. Mag. 85 (2005) 3767–3794.
[27] A.R.Allnatt, A.B.Lidiard, Atomic Transport in Solids, Cambridge University Press, 2003.
[28] T.R.Anthony, in:, Diffus. Solids, Elsevier, 1975, pp. 353–379.
[29] A.Van derVen, G.Ceder, M.Asta, P.D.Tepesch, Phys. Rev. B 64 (2001) 184307.
[30] A.Van derVen, Acta Mater. 52 (2004) 1223–1235.
[31] M.A.Abd-Elhady, G.A.Sargent, J. Mater. Sci. 21 (1986) 2657–2663.
[32] M.A.Abd-Elhady, G.A.Sargent, J. Mater. Sci. 21 (1986) 3643–3647.
[33] L.P.Lehman, T.H.Kosel, MRS Proc. 39 (1984) 147.
[34] G.A.Young, D.R.Eno, Fontevraud 8 (2014).

FIGURE CAPTION

Figure 1. Plots showing the temperature dependence of Ni self-diffusion coefficient in dilute Ni alloys with various composition of impurity (a) P, (b) S, (c) Si, and (d) Al from 0 to 1 at.%.

Figure 2. Plots showing the temperature dependence of effective vacancy diffusion coefficient in dilute Ni alloys with various composition of impurity (a) P, (b) S, (c) Si, and (d) Al from 0 to 1 at.% . The two vacancy diffusion limits by free vacancies and vacancy-solute pairs are plotted by ○ and ◊, respectively.

Figure 3. Schematic plot showing the three special quasi-random structures (SQS) of the $2 \times 2 \times 2$ fcc supercell consisting of 20 Ni atoms, 10 Cr atoms, 1 impurity atom, and 1 vacancy. The Ni, Cr, and impurity atoms are displayed as blue, light red, and pink spheres, and the vacancy is the square labeled as "Vac". The four spheres labeled by the element name with number are the atoms in the nearest-neighbor distance with the impurity atom and vacancy. (b) Column plots showing the vacancy binding of 3*sp* impurities in the concentrated SQS and dilute Ni, and (c) Plots showing the averaged change of migration barrier (with standard deviation) of the exchange (ω_2-type) hop and rotation (ω_1-type) hops associated with the addition of the 3*sp* impurity atom in the concentrated SQS.

TABLE CAPTION

Table 1. Bader charges of the impurity atom in the dilute Ni and concentrated SQS at the ground state (GS) and transition state (TS) of the ω_1 and ω_2 hops. The plus-minus sign shows the standard deviation of the collected data.

Table 1. Bader charges of the impurity atom in the dilute Ni and concentrated SQS at the ground state (GS) and transition state (TS) of the ω_1 and ω_2 hops. The plus-minus sign shows the standard deviation of the collected data.

	GS (Ni)	GS (SQS)	TS-ω_1(Ni)	TS-ω_1 (SQS)	TS-ω_2(Ni)	TS-ω_2 (SQS)
P	−0.29 *e*	−0.55 (±0.030)	−0.25 *e*	−0.55 (±0.053)	−0.06 *e*	−0.38 (±0.016)
S	−0.40 *e*	−0.76 (±0.035)	−0.60 *e*	−0.80 (±0.045)	−0.46 *e*	−0.68 (±0.019)
Si	+0.42 *e*	+0.11 (±0.029)	+0.48 *e*	+0.14 (±0.062)	+0.73 *e*	+0.38 (±0.057)
Al	+1.85 *e*	+1.62 (±0.035)	+1.86 *e*	+1.62 (±0.048)	+1.79 *e*	+1.60 (±0.034)

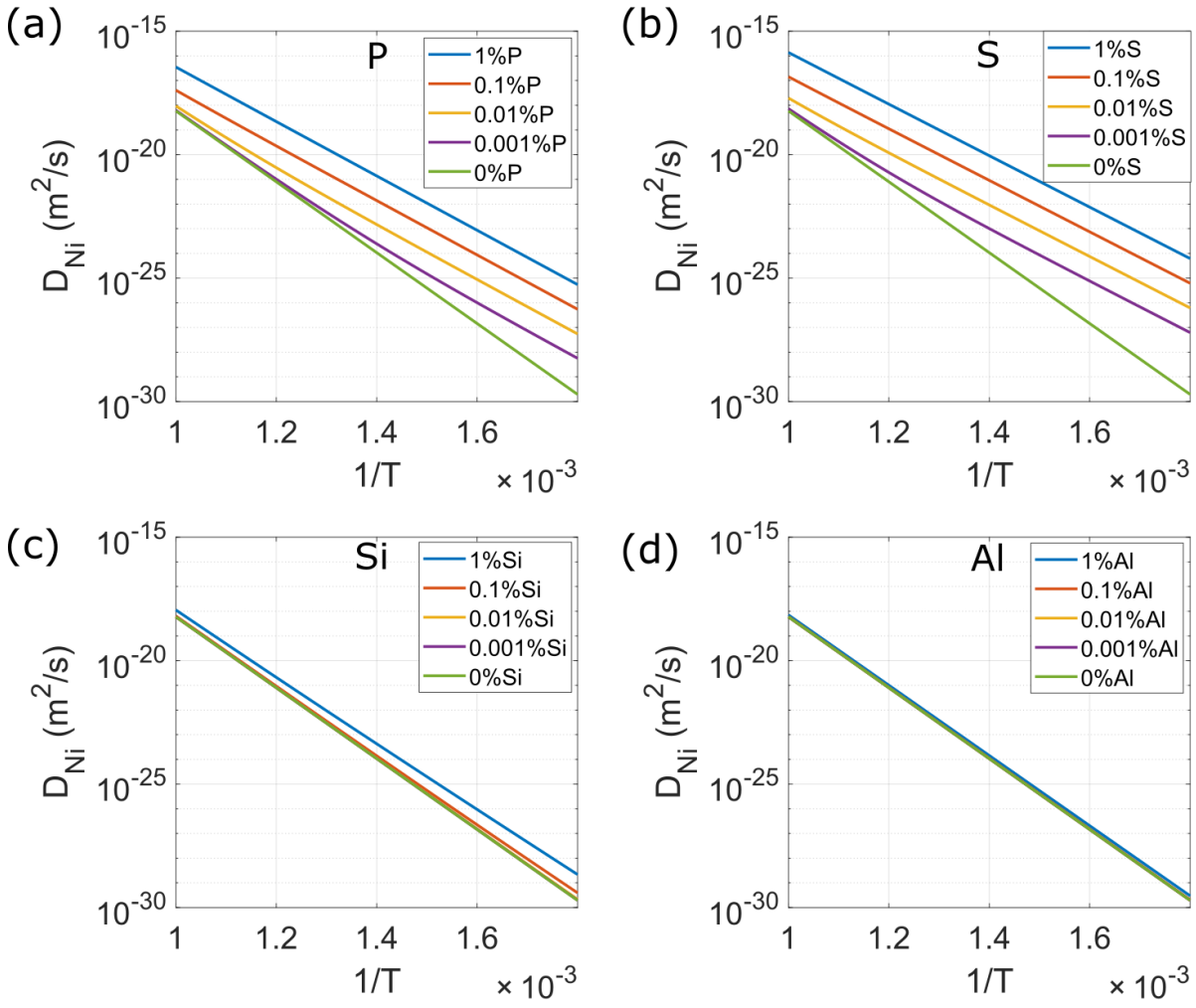

Figure 1. Plots showing the temperature dependence of Ni self-diffusion coefficient in dilute Ni alloys with various composition of impurity (a) P, (b) S, (c) Si, and (d) Al from 0 to 1 at.%.

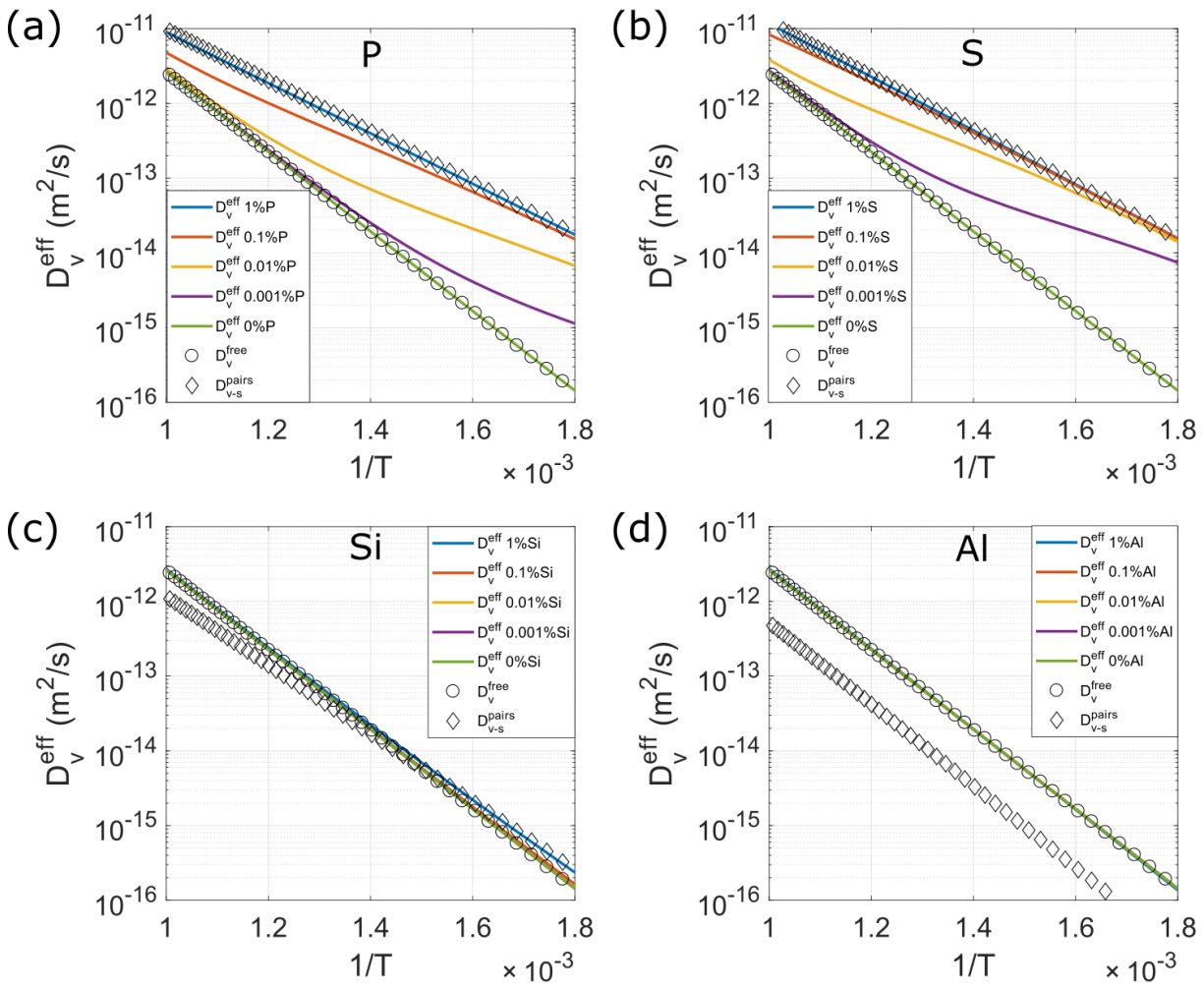

Figure 2. Plots showing the temperature dependence of effective vacancy diffusion coefficient in dilute Ni alloys with various composition of impurity (a) P, (b) S, (c) Si, and (d) Al from 0 to 1 at.% . The two vacancy diffusion limits by free vacancies and vacancy-solute pairs are plotted by ○ and ◊, respectively.

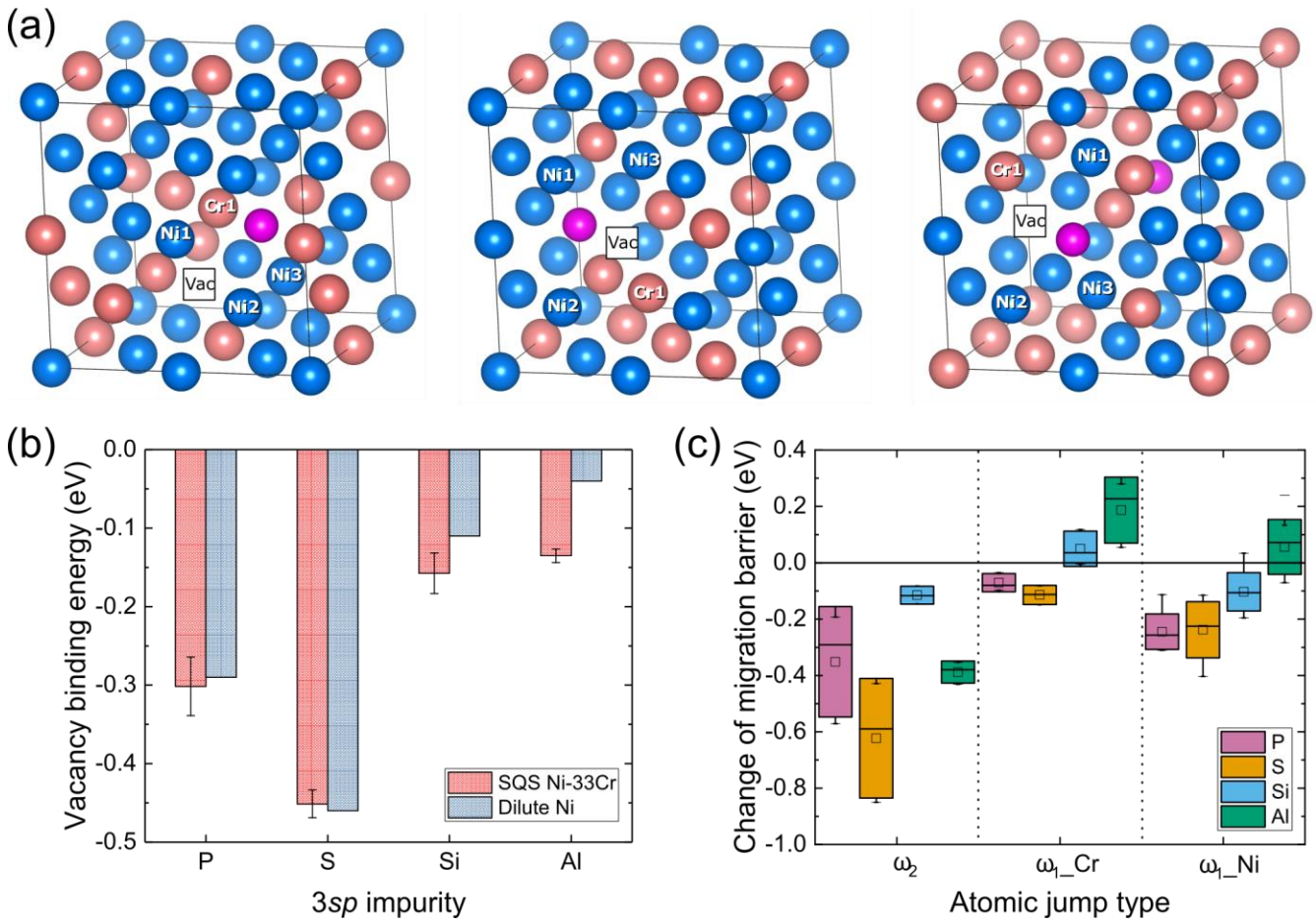

Figure 3. (a) Schematic plot showing the three special quasi-random structures (SQS) of the 2 × 2 × 2 fcc supercell consisting of 20 Ni atoms, 10 Cr atoms, 1 impurity atom, and 1 vacancy. The Ni, Cr, and impurity atoms are displayed as blue, light red, and pink spheres, and the vacancy is the square labeled as "Vac". The four spheres labeled by the element name with number are the atoms in the nearest-neighbor distance with the impurity atom and vacancy. (b) Column plots showing the vacancy binding of 3*sp* impurities in the concentrated SQS and dilute Ni, and (c) Plots showing the averaged change of migration barrier (with standard deviation) of the exchange (ω_2-type) hop and rotation (ω_1-type) hops associated with the addition of the 3*sp* impurity atom in the concentrated SQS.

Figure 1

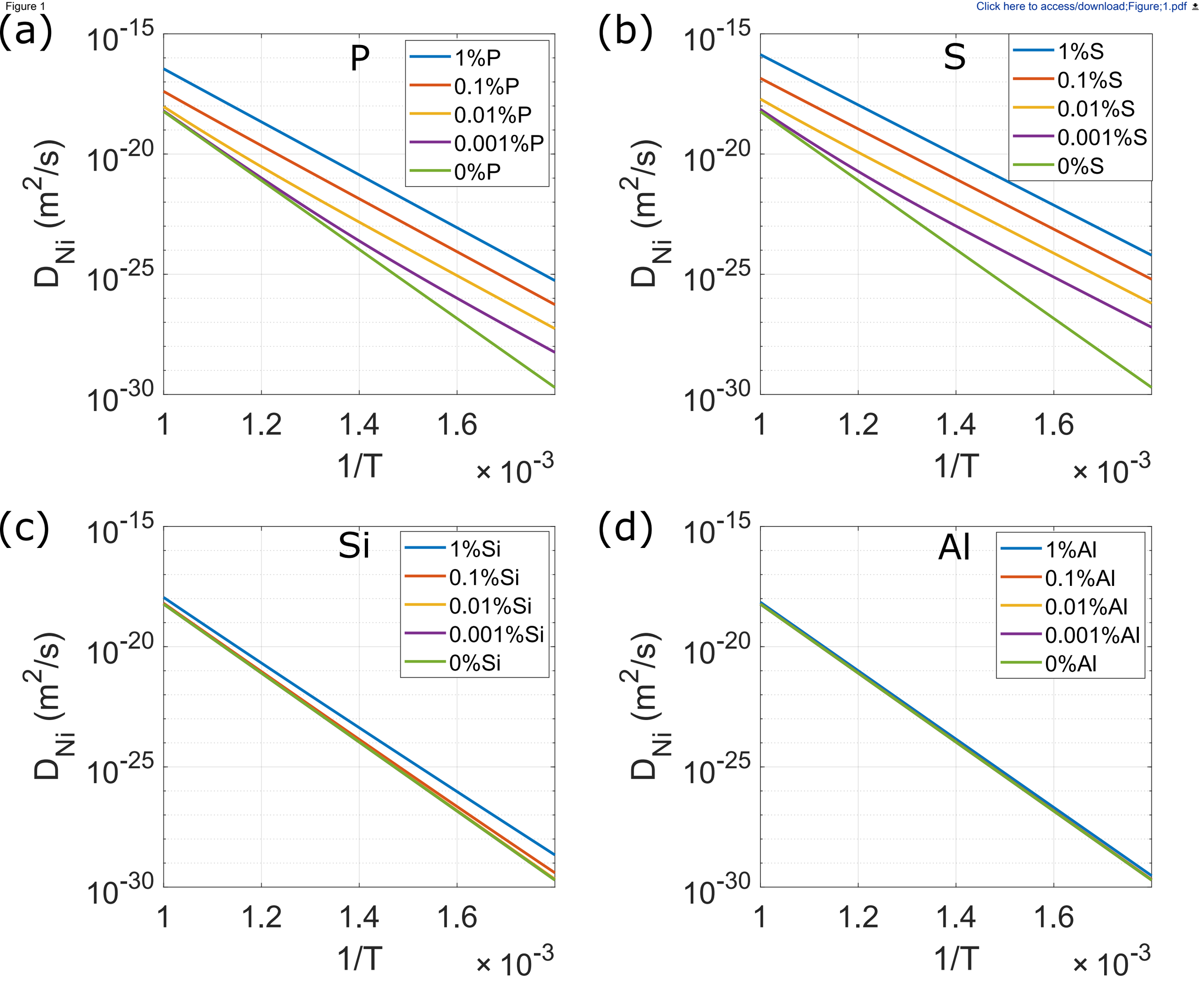

Figure 2

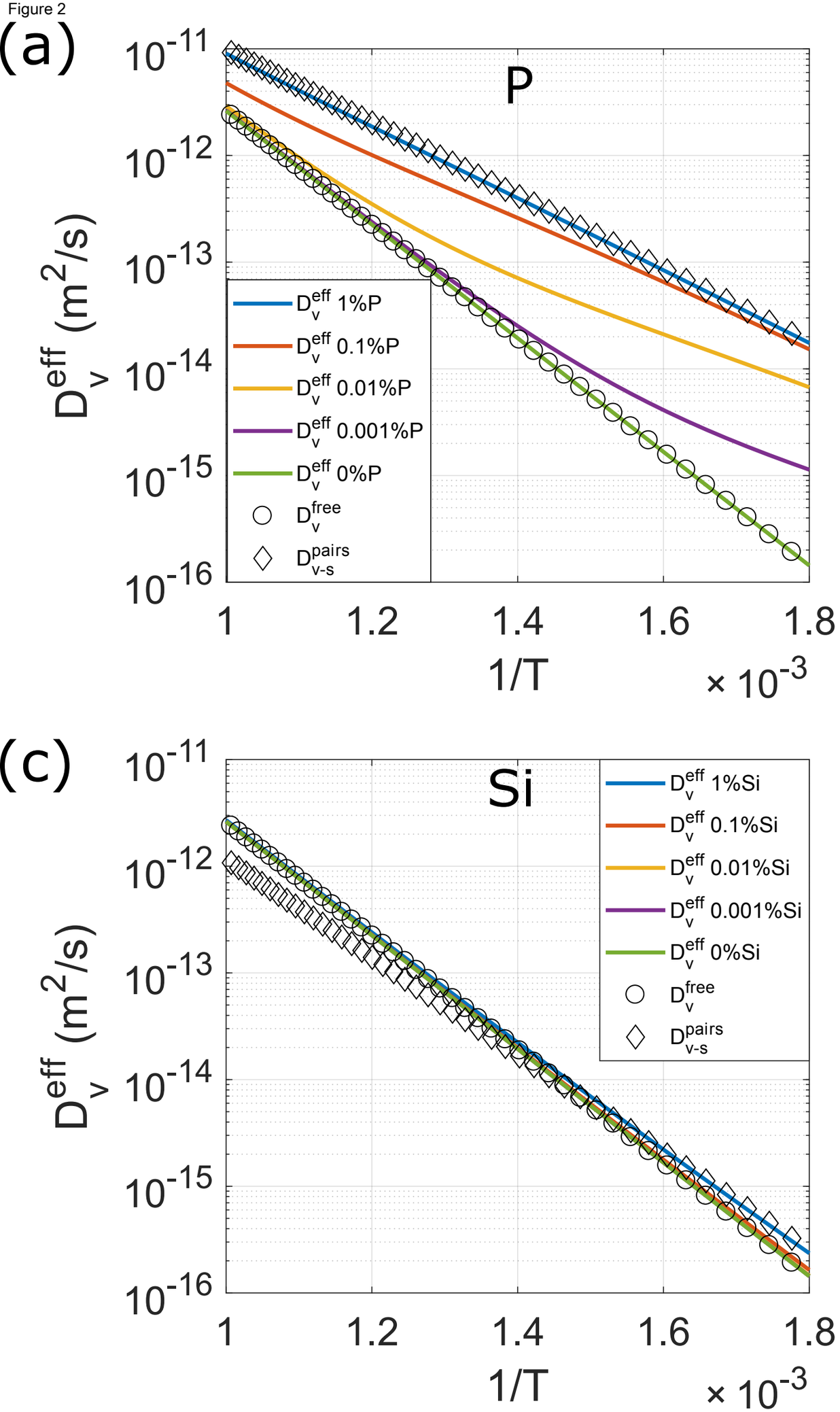

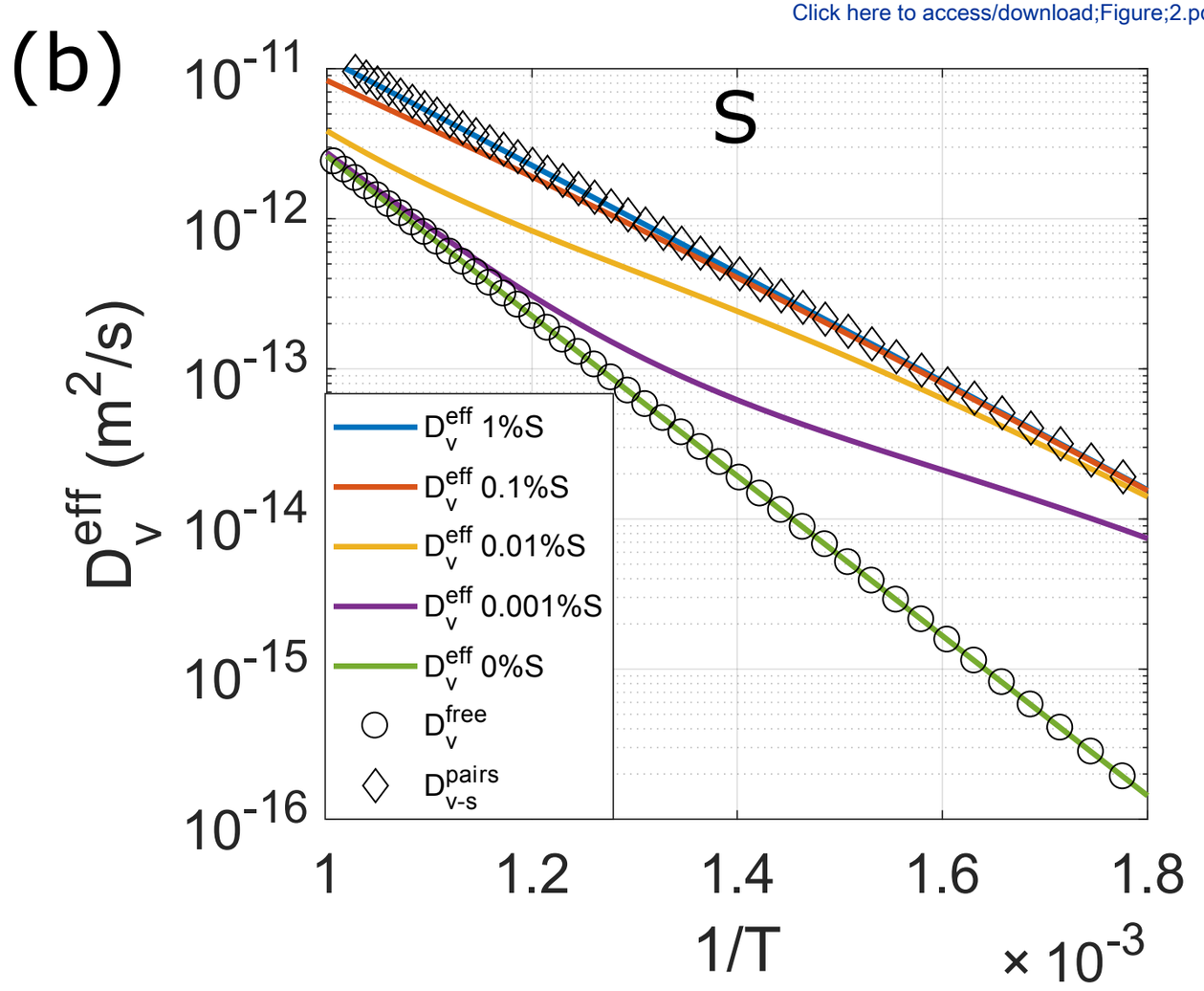

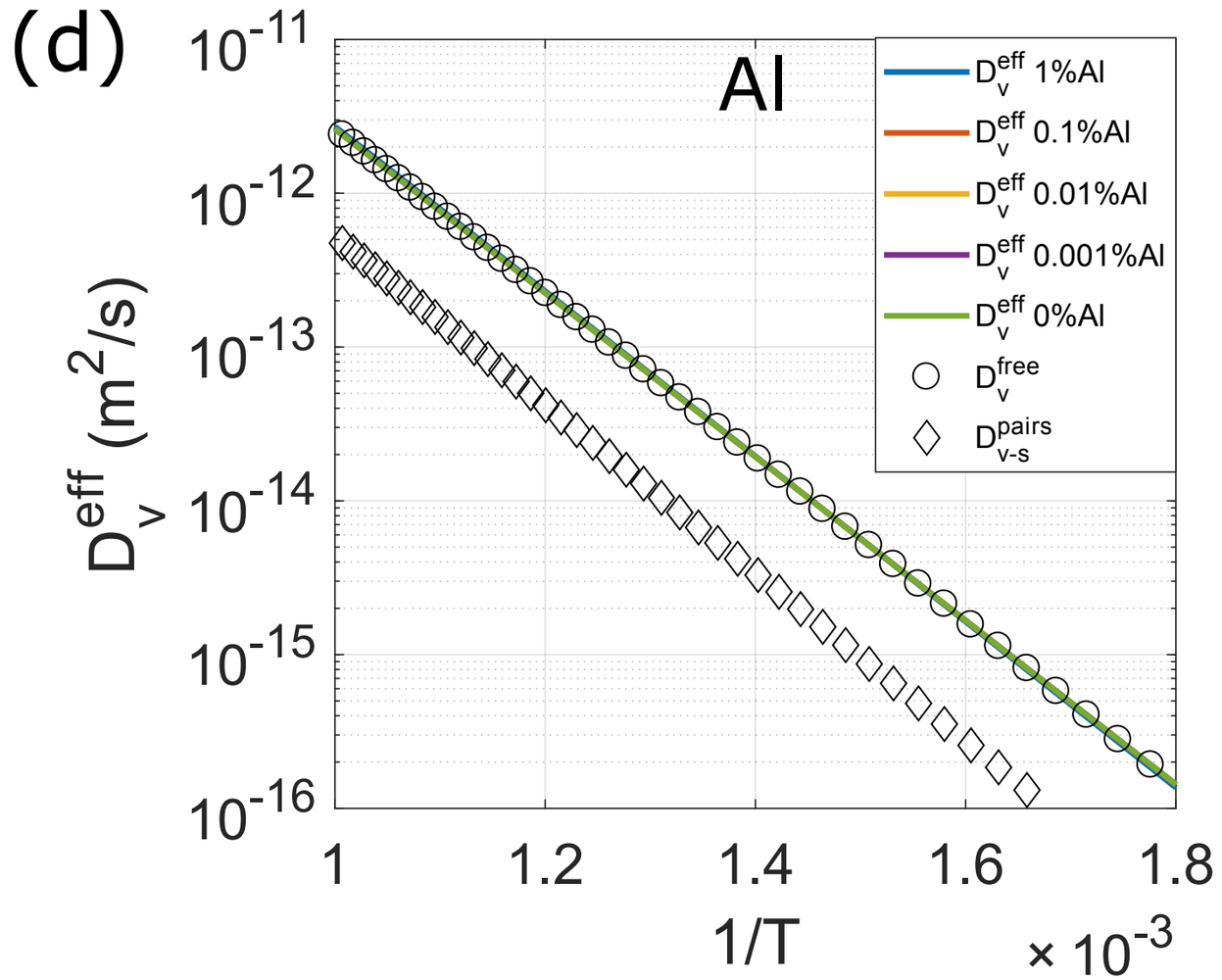

Figure 3

Click here to access/download;Figure;3.png